

Spin-dependent inelastic collisions in spin-2 Bose-Einstein condensates

Satoshi Tojo,¹ Taro Hayashi,¹ Tatsuyoshi Tanabe,¹ Takuya Hirano,¹ Yuki Kawaguchi,² Hiroki Saito,³ and Masahito Ueda^{2,4}

¹*Department of Physics, Gakushuin University, Tokyo 171-8588, Japan*

²*Department of Physics, University of Tokyo, Tokyo 113-0033, Japan*

³*Department of Applied Physics and Chemistry, University of Electro-Communications, Tokyo 182-8585, Japan*

⁴*ERATO Macroscopic Quantum Project, JST, Tokyo 113-8656, Japan*

(Received 7 July 2009; published 12 October 2009)

We studied spin-dependent two-body inelastic collisions in $F=2$ ^{87}Rb Bose-Einstein condensates both experimentally and theoretically. The ^{87}Rb condensates were confined in an optical trap and selectively prepared in various spin states in the $F=2$ manifold at a magnetic field of 3.0 G. The measured atom loss rates depend on the spin states of colliding atoms. We measured two fundamental loss coefficients for two-body inelastic collisions with total spins of 0 and 2. The loss coefficients determine the loss rates of all the spin pairs. The experimental results for mixtures of all spin combinations are in good agreement with numerical solutions of the Gross-Pitaevskii equations that include the effect of a magnetic field gradient.

DOI: [10.1103/PhysRevA.80.042704](https://doi.org/10.1103/PhysRevA.80.042704)

PACS number(s): 34.50.-s, 03.75.Mn, 03.75.Kk

I. INTRODUCTION

The field of cold collisions has attracted extensive interest and has grown explosively since the early days of atom cooling and trapping [1]. The development of novel techniques for cooling and manipulating atoms have led to a deeper understanding of physics of collisions: e.g., evaporative cooling enabled Bose-Einstein condensates (BECs) to be realized and opened the field of ultracold collisions, while the evaporative cooling process itself relies on the nature of collisions. The mean-field theory of BEC, which successfully describes the properties of BEC, depends on the elastic s -wave scattering length to characterize the atomic interaction energy [1,2]. Inelastic collisions also play important roles, e.g., in cooling and retaining an atomic or molecular cloud in a trap [3–10].

In an optical trap, the spin degrees of freedom of atoms are liberated enabling a rich variety of spinor BECs physics to be studied. Spin-2 BECs have attracted much interest in recent years and there have been several experimental studies of spin-2 systems, including investigations of their magnetic phases [6–9], of multiply charged vortices [11], and the phase separation between spin-2 and spin-1 BECs [12,13]. It is, however, difficult to observe stationary states of these phenomena because the ^{85}Rb $F=2$ BEC has a negative scattering length, and in ^7Li , ^{23}Na , ^{39}K , and ^{87}Rb the $F=2$ states are in the upper hyperfine manifold. Ultracold gases in the upper hyperfine states decay to the lower hyperfine state. ^{87}Rb atoms are highly suitable for investigating the properties of a spin-2 BEC because they have much lower inelastic collision rates than other species; e.g., ^{87}Rb has a loss rate of the order of 10^{-14} cm^3/s , which is much lower than that of ^{23}Na [5].

In this paper, we systematically investigate ultracold two-body inelastic collisions between Zeeman states of $F=2$ atoms both experimentally and theoretically. The experiment was conducted by creating an $F=2$ spinor ^{87}Rb BEC in an optical trap and populating desired Zeeman sublevels by radio-frequency transitions. We measured the atom loss rates for various initial populations. Spin-exchange collisions were negligible at a bias magnetic field of 3.0 G. By analogy with

the scattering length in elastic collisions, two-body inelastic collisions are described by two parameters, b_0 and b_2 , which correspond to channels with the total spins of 0 and 2, respectively. We experimentally determine these two parameters from the loss rates of single-component BECs of $|F=2, m_F=1\rangle$ and $|F=2, m_F=0\rangle$. We also measured the atom loss rates for two-component BECs of all possible sets of magnetic sublevels and we compared the results with our theoretical model. We calculated the time evolution of the number of atoms in two-component BECs using the values of b_0 and b_2 obtained by two methods: the single-mode approximation (SMA) and the Gross-Pitaevskii (GP) equations that include the effect of a magnetic field gradient. The results obtained with the latter method agreed well with the experimental results.

II. THEORY OF TWO-BODY INELASTIC COLLISIONS

We first consider a system of spin-2 ^{87}Rb atoms with no atom losses. The Hamiltonian for this system is given by

$$\hat{H} = \sum_{m=-2}^2 \int d\mathbf{r} \hat{\psi}_m^\dagger(\mathbf{r}) \left[-\frac{\hbar^2}{2M} \nabla^2 + V_m(\mathbf{r}) \right] \hat{\psi}_m(\mathbf{r}) + \hat{H}_{\text{int}}, \quad (1)$$

where $\hat{\psi}_m$ and V_m are the field operator and an external potential for the hyperfine state $|F=2, m\rangle$, and M is the mass of the ^{87}Rb atoms. The interaction Hamiltonian \hat{H}_{int} has the form [14]

$$\hat{H}_{\text{int}} = \sum_{\mathcal{F}=0,2,4} g_{\mathcal{F}} \sum_{M=-\mathcal{F}}^{\mathcal{F}} \int d\mathbf{r} \hat{A}_{\mathcal{F}\mathcal{M}}^\dagger(\mathbf{r}) \hat{A}_{\mathcal{F}\mathcal{M}}(\mathbf{r}), \quad (2)$$

where

$$g_{\mathcal{F}} = \frac{4\pi\hbar^2 a_{\mathcal{F}}}{M}, \quad (3)$$

with $a_{\mathcal{F}}$ being the s -wave scattering length with the colliding channel of total spin \mathcal{F} and $\hat{A}_{\mathcal{F}\mathcal{M}}$ is the annihilation operator of two atoms with total spin $|\mathcal{F}, M\rangle$ defined as

$$\hat{A}_{\mathcal{F}\mathcal{M}}(\mathbf{r}) = \sum_{m,m'=-2}^2 C_{mm'}^{\mathcal{F}\mathcal{M}} \hat{\psi}_m(\mathbf{r}) \hat{\psi}_{m'}(\mathbf{r}) \quad (4)$$

with $C_{mm'}^{\mathcal{F}\mathcal{M}} \equiv \langle \mathcal{F}, M | 2, m; 2, m' \rangle$ being the Clebsch-Gordan coefficient.

We take into account only the two-body inelastic loss, since the two-body inelastic collision is the dominant atom loss process for the upper hyperfine state of ^{87}Rb atoms. We neglect the three-body losses and density-independent losses, such as background-gas scattering and photon scattering. The two-body inelastic collision changes the hyperfine spin of either or both of the colliding atoms from $F=2$ to $F=1$. Consequently, the colliding atoms acquire a kinetic energy corresponding to the hyperfine splitting, allowing them to escape from the trap.

We write the master equation for the time evolution of the system with two-body inelastic loss as

$$\frac{\partial \hat{\rho}}{\partial t} = \frac{1}{i\hbar} [\hat{H}, \hat{\rho}] + \left(\frac{\partial \hat{\rho}}{\partial t} \right)_{\text{loss}}, \quad (5)$$

where $\hat{\rho}$ represents the density operator for the atoms in the $F=2$ manifold. The second term on the right-hand side of Eq. (5) describes the atom loss, which must be rotationally invariant. If we assume that the atoms after the two-body inelastic collision immediately escape from the system and do not interact with the other atoms, the atomic-loss part of the master equation can be written as [15]

$$\left(\frac{\partial \hat{\rho}}{\partial t} \right)_{\text{loss}} = \sum_{\mathcal{F}=0,2} \frac{b_{\mathcal{F}}}{4} \sum_{\mathcal{M}=-\mathcal{F}}^{\mathcal{F}} \int d\mathbf{r} [2\hat{A}_{\mathcal{F}\mathcal{M}}(\mathbf{r}) \hat{\rho} \hat{A}_{\mathcal{F}\mathcal{M}}^{\dagger}(\mathbf{r}) - \hat{A}_{\mathcal{F}\mathcal{M}}^{\dagger}(\mathbf{r}) \hat{A}_{\mathcal{F}\mathcal{M}}(\mathbf{r}) \hat{\rho} - \hat{\rho} \hat{A}_{\mathcal{F}\mathcal{M}}^{\dagger}(\mathbf{r}) \hat{A}_{\mathcal{F}\mathcal{M}}(\mathbf{r})], \quad (6)$$

where the constant $b_{\mathcal{F}}$ characterizes the loss rate for colliding channel with total spin \mathcal{F} . We note that Eq. (6) is rotationally invariant. If the dipolar decay is negligible, the total spin \mathcal{F} before and after the collision must be the same, and therefore, inelastic decay through the $\mathcal{F}=4$ channel is prohibited in Eq. (6): this is experimentally confirmed in the following section.

For example, let us consider a mixture of $|2, 0\rangle$ and $|2, 1\rangle$ atoms. Using Eq. (6), we obtain the two-body inelastic loss of the $|2, 0\rangle$ component as

$$\begin{aligned} \left(\frac{\partial}{\partial t} \langle \hat{\psi}_0^{\dagger} \hat{\psi}_0 \rangle \right)_{\text{loss}} &= \text{Tr} \left[\left(\frac{\partial \hat{\rho}}{\partial t} \right)_{\text{loss}} \hat{\psi}_0^{\dagger} \hat{\psi}_0 \right] = - \left(\frac{1}{5} b_0 + \frac{2}{7} b_2 \right) \\ &\times \langle \hat{\psi}_0^{\dagger 2} \hat{\psi}_0^2 \rangle - \frac{1}{7} b_2 \langle \hat{\psi}_0^{\dagger} \hat{\psi}_0 \hat{\psi}_1^{\dagger} \hat{\psi}_1 \rangle, \end{aligned} \quad (7)$$

where Tr represents the trace. In the mean-field approximation, Eq. (7) is simplified as

$$\frac{dn_0(\mathbf{r})}{dt} = -K_2^{(0,0)} n_0^2(\mathbf{r}) - K_2^{(0,1)} n_0(\mathbf{r}) n_1(\mathbf{r}), \quad (8)$$

where $K_2^{(0,0)} = b_0/5 + 2b_2/7$, $K_2^{(0,1)} = b_2/7$, and n_m is the density of component m . In general, two-body inelastic decay in a two-component mixture has the form

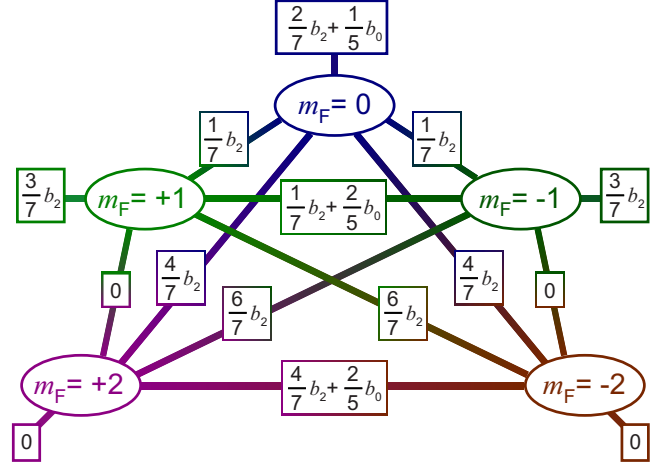


FIG. 1. (Color online) Inelastic collision rates $K_2^{(m,m')}$ for all combinations of m and m' in a spin-2 BEC. A rectangle that connects two ellipses corresponds to a collision between two different components, whereas a rectangle linked to one ellipse corresponds to a collision between the same component.

$$\frac{dn_m(\mathbf{r})}{dt} = -K_2^{(m,m)} n_m^2(\mathbf{r}) - K_2^{(m,m')} n_m(\mathbf{r}) n_{m'}(\mathbf{r}), \quad (9)$$

and for a single-component system,

$$\frac{dn_m(\mathbf{r})}{dt} = -K_2^{(m,m)} n_m^2(\mathbf{r}). \quad (10)$$

The coefficients $K_2^{(m,m')}$ for all m and m' are shown in Fig. 1.

From Eq. (5), the equation of motion for $\langle \hat{\psi}_m \rangle$ is given by

$$\frac{\partial}{\partial t} \langle \hat{\psi}_m(\mathbf{r}) \rangle = \frac{1}{i\hbar} \langle [\hat{\psi}_m(\mathbf{r}), \hat{H}] \rangle + \text{Tr} \left[\left(\frac{\partial \rho}{\partial t} \right)_{\text{loss}} \hat{\psi}_m(\mathbf{r}) \right]. \quad (11)$$

Using Eq. (6), the second term on the right-hand side of Eq. (11) can be rewritten as

$$\sum_{\mathcal{F}=0,2} \frac{b_{\mathcal{F}}}{4} \sum_{\mathcal{M}=-\mathcal{F}}^{\mathcal{F}} \int d\mathbf{r}' \langle [\hat{A}_{\mathcal{F}\mathcal{M}}^{\dagger}(\mathbf{r}') \hat{A}_{\mathcal{F}\mathcal{M}}(\mathbf{r}') \hat{\psi}_m(\mathbf{r})] \rangle. \quad (12)$$

We find that Eq. (12) has the same form as $\langle [\hat{H}_{\text{int}}, \hat{\psi}_m] \rangle$ with $g_{\mathcal{F}}$ being replaced by $b_{\mathcal{F}}/2$. In the mean-field theory, we thus expect that the two-body loss can be incorporated into the GP equation by replacing $g_{\mathcal{F}}$ with $g_{\mathcal{F}} - i\hbar b_{\mathcal{F}}/2$. Thus, the GP equation for a spin-2 BEC with two-body loss is obtained as

$$\begin{aligned} i\hbar \frac{\partial \psi_m}{\partial t} &= \left(-\frac{\hbar^2}{2M} \nabla^2 + V_m \right) \psi_m \\ &+ \sum_{\mathcal{F}=0,2,4} \tilde{g}_{\mathcal{F}} \sum_{\mathcal{M}=-\mathcal{F}}^{\mathcal{F}} \sum_{m_1, m_2, m_3} C_{mm_1}^{\mathcal{F}\mathcal{M}} C_{m_2 m_3}^{\mathcal{F}\mathcal{M}} \psi_{m_1}^* \psi_{m_2} \psi_{m_3}, \end{aligned} \quad (13)$$

where

$$\tilde{g}_0 = g_0 - \frac{i\hbar b_0}{2}, \quad \tilde{g}_2 = g_2 - \frac{i\hbar b_2}{2}, \quad \tilde{g}_4 = g_4. \quad (14)$$

If we assume that the atom density $n_m(\mathbf{r}, t)$ of a single-component BEC always follows the Thomas-Fermi profile,

$$n_m(\mathbf{r}, t) = \frac{M}{4\pi\hbar^2 a_m} [\mu(t) - V(\mathbf{r})], \quad (15)$$

where a_m is the scattering length for component m and $\mu(t)$ is determined from

$$N_m(t) = \int n_m(\mathbf{r}, t) d\mathbf{r}, \quad (16)$$

we can integrate Eq. (10), giving [3,9]

$$\frac{dN_m(t)}{dt} = -\gamma_m K_2^{(m,m)} N_m^{7/5}(t). \quad (17)$$

Here the coefficient γ_m is given by

$$\gamma_m = \frac{15^{2/5}}{14\pi} \left(\frac{M\bar{\omega}}{\hbar\sqrt{a_m}} \right)^{6/5} \quad (18)$$

with $\bar{\omega}$ being the average trap frequency. The solution of Eq. (17) is obtained as

$$N_m(t) = \frac{5^{5/2}}{[5N_m^{-2/5}(0) + 2\gamma_m K_2^{(m,m)} t]^{5/2}}. \quad (19)$$

For a two-component system, we assume that both components m and m' have identical density profiles that are given by

$$n_m(\mathbf{r}, t) = \frac{M}{4\pi\hbar^2 \bar{a}} \rho_m(t) [\mu(t) - V(\mathbf{r})], \quad (20)$$

$$n_{m'}(\mathbf{r}, t) = \frac{M}{4\pi\hbar^2 \bar{a}} \rho_{m'}(t) [\mu(t) - V(\mathbf{r})], \quad (21)$$

where \bar{a} is the arithmetic average of the three scattering lengths (between m - m , m' - m' , and m - m'), $\rho_{m(m')}(t) = N_{m(m')}(t)/N(t)$, and $\mu(t)$ is determined from

$$N(t) = \int [n_m(\mathbf{r}, t) + n_{m'}(\mathbf{r}, t)] d\mathbf{r}. \quad (22)$$

We also assume that the coherent spin dynamics is negligible. Such an SMA is accurate if the three scattering lengths are the same. Integrating Eq. (9), we obtain

$$\frac{dN_m(t)}{dt} = -\bar{\gamma} N^{7/5}(t) [K_2^{(m,m)} \rho_m^2(t) + K_2^{(m,m')} \rho_m(t) \rho_{m'}(t)], \quad (23)$$

where $\bar{\gamma}$ has the same form as Eq. (18) in which a_m is replaced by \bar{a} .

III. EXPERIMENTAL SETUP

The experimental apparatus and procedure to create ^{87}Rb condensates are almost the same as in our previous study [6,9]. A precooled thermal cloud prepared by the first magneto-optical trap (MOT) was transferred to the second MOT by irradiating the first MOT with a weak near-resonant

cw laser beam focused on the center of the MOT. Over 10^9 atoms in the second MOT were optically pumped into the $|2, +2\rangle$ state and recaptured in an Ioffe-Pritchard (clover-leaf) magnetic trap. A BEC containing 10^6 atoms was created by evaporative cooling with frequency sweeping an rf field for 18 s.

The BEC was loaded into a crossed far-off-resonance optical trap (FORT) at a wavelength of 850 nm. One of the laser beams propagated along the long axis of the cigar-shaped BEC and had a power of 7 mW and a $1/e^2$ radius at the focus of 31 μm . The other laser beam had a power of 11 mW and a beam waist of 97 μm and was focused on and crossed the first beam. The potential depth of the crossed FORT was estimated to be about 1 μK . Both lasers had power fluctuations of less than 1%. The radial (axial) trap frequency measured from the parametric resonance [16] was $2\pi \times 162$ Hz ($2\pi \times 21$ Hz). The average trap frequency determined by measuring the parametric resonance was $2\pi \times 82$ Hz, which was consistent with that determined by measuring the release energy [17].

The condensed atoms in the $|2, +2\rangle$ state in the magnetic trap were transferred to the crossed FORT. The magnetic trap was quickly turned off and the quantization axis was then nonadiabatically inverted. The condensed atoms were kept in the trap for 200 ms. In the way, condensates containing 3.2×10^5 atoms in the $|2, -2\rangle$ state were prepared in the crossed FORT. Some of the condensed atoms in the $|2, -2\rangle$ state can be transferred to desired spin states $|2, m_F\rangle$ by the Landau-Zener transition with an external magnetic field of 20.5 G [18]. In this magnetic field, the condensed atoms can be selectively transferred to the desired target states by quadratic Zeeman shifts. The relative populations of $|2, m_F\rangle$ states were controlled by the rf field strength and the sweep rate. The observed fluctuation in the number of atoms was estimated to be 10%, which was due to variations in the initial number of BEC atoms and in the rf-transfer rate between spin states. After state preparation, the 20.5 G field was turned off and an accurately controlled external magnetic field of 3.0 G was immediately applied. The crossed FORT was turned off at the end of the time evolution period, and absorption imaging was performed after a free expansion time of 15 ms to measure the population distribution of each spin component by the Stern-Gerlach method [17]. A magnetic field fluctuation of ~ 10 mG was measured by observing the transfer rate for magnetic-dipole transitions and the residual gradient magnetic field was estimated to be ~ 30 mG/cm [6].

IV. RESULTS AND DISCUSSION

Figure 2 plots the time dependence of the number of atoms of a single-component BEC initially prepared in the $|2, 0\rangle$ (filled circles), $|2, -1\rangle$ (open squares), and $|2, -2\rangle$ states (open triangles). Each point represents an average typically over four samples. The observed condensate fraction was greater than 90% and the temperature of the thermal cloud was below 100 nK. In the measurement, finite temperature effects in the condensates, as seen in Ref. [19], were not observed. The relative population of the initially prepared single component was observed to be larger than 0.95

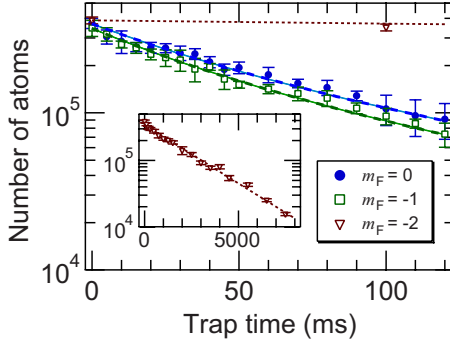


FIG. 2. (Color online) Time dependence of the number of atoms in a single-component BEC initially prepared in $|2,0\rangle$ (filled circles), $|2,-1\rangle$ (open squares), and $|2,-2\rangle$ (open triangles) states. The inset shows the decay of $|2,-2\rangle$ atoms for a longer period. The experimental data are fitted by Eq. (17) (dashed lines). The theoretical curves are calculated from the GP equation (solid lines).

through the time evolution since a magnetic field strength of 3.0 G suppressed the spin-exchange collisions and only the initially prepared single component was observed through the time evolution [6]. The quadratic Zeeman energies between $|2,0\rangle$ and $|2,\pm 1\rangle$ and between $|2,0\rangle$ and $|2,\pm 2\rangle$ were 31 nK and 124 nK, respectively. The number of atoms in $|2,0\rangle$ and $|2,-1\rangle$ states decreased rapidly with time. By contrast, the number of atoms in the $|2,-2\rangle$ state remained almost unchanged within 100 ms, showing good agreement with the collision rate $K_2^{(-2,-2)}=0$. The value of the one-body

loss coefficient K_1 is experimentally estimated to be $K_1=0.4\text{ s}^{-1}$ from the result for the $|2,-2\rangle$ state (see the inset of Fig. 2), and the three-body rate constant K_3 was deduced by Söding *et al.* [3] to be $K_3=1.8\times 10^{-29}\text{ cm}^6\text{ s}^{-1}$. In our experimental condition, the contributions of the K_1 and K_3 terms to the atom loss are negligible compared with that of the K_2 term. Therefore, the decays in the number of atoms for the $|2,0\rangle$ and $|2,-1\rangle$ atoms are well fitted by Eq. (17) based on SMA calculation. The inelastic collision rates are thus obtained as $K_2^{(0,0)}=(8.9\pm 0.9)\times 10^{-14}\text{ cm}^3/\text{s}$ and $K_2^{(-1,-1)}=(10.4\pm 1.0)\times 10^{-14}\text{ cm}^3/\text{s}$ for $m_F=0$ and $m_F=-1$, respectively. From these values of $K_2^{(0,0)}=b_0/5+2b_2/7$ and $K_2^{(-1,-1)}=3b_2/7$, we deduce the inelastic collision coefficients $b_2=(24.3\pm 2.4)\times 10^{-14}\text{ cm}^3/\text{s}$ and $b_0=(9.9\pm 5.5)\times 10^{-14}\text{ cm}^3/\text{s}$ with scattering lengths of $94.57a_B$ for $m_F=0$ and $95.68a_B$ for $m_F=-1$ with a_B being the Bohr radius, respectively [8]. We also calculated the time evolution using the GP equations with the above values to compare the results obtained using the GP equations with those obtained using the SMA. The difference between the results obtained by GP and SMA calculations is negligibly small as shown in Fig. 2.

We next consider the loss of a two-component mixture to check the consistency of Fig. 1 combined with the measured values of b_0 and b_2 . We observed atom losses for all pairs of spin states with initially equal populations as shown in Fig. 3. The atom loss rates depend strongly on the spin states of colliding atoms. We first discuss the atom loss rate for the $(2,-1)+(2,-2)$ pair. As Fig. 3(a) shows, the number of

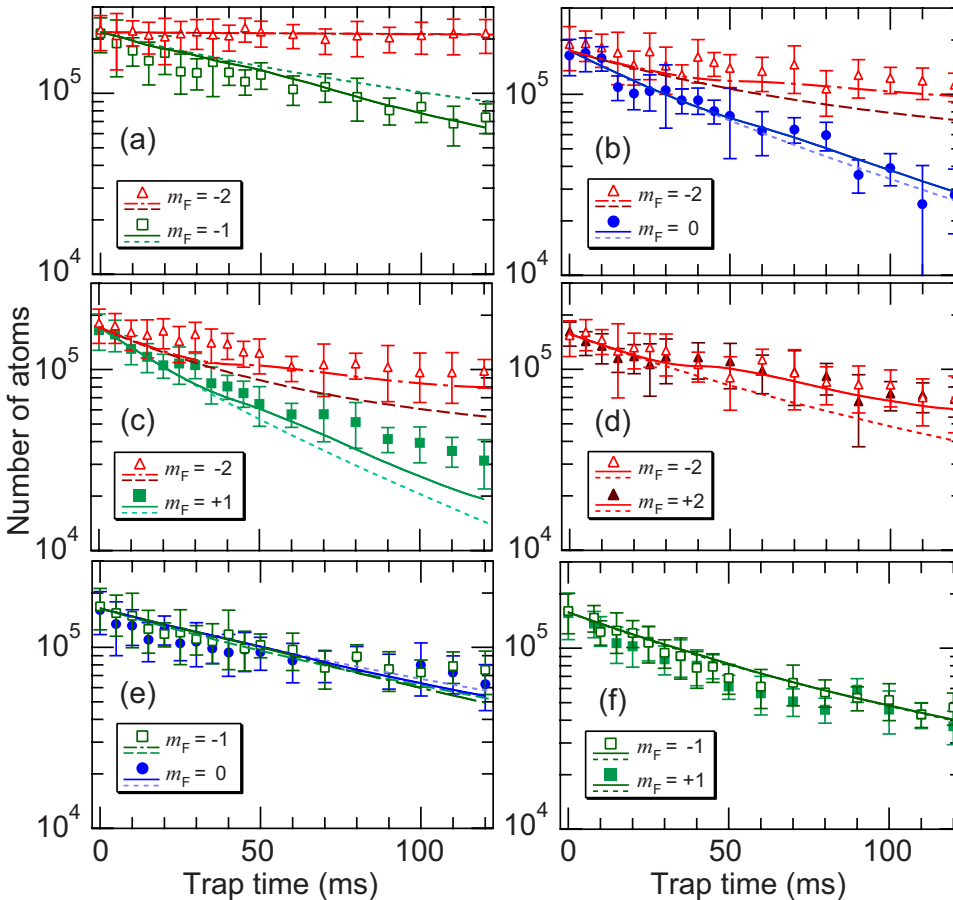


FIG. 3. (Color online) Time dependence of numbers of condensed atoms for various initially populated spin states (a) $(2,-1)+(2,-2)$, (b) $(2,0)+(2,-2)$, (c) $(2,+1)+(2,-2)$, (d) $(2,+2)+(2,-2)$, (e) $(2,0)+(2,-1)$, and (f) $(2,+1)+(2,-1)$ pairs. The theoretical curves are calculated from Eq. (23) with the SMA (dotted and dashed lines) or the GP equations that include the effect of a magnetic field gradient (solid and dot-dashed lines).

$|2, -2\rangle$ atoms remained almost unchanged even in the presence of $|2, -1\rangle$ atoms. This is consistent with the prediction $K_2^{(-1,-2)} = K_2^{(-2,-2)} = 0$ as shown in Fig. 1. On the other hand, for $(2, 0) + (2, -2)$, $(2, +1) + (2, -2)$, and $(2, +2) + (2, -2)$ pairs, the $|2, -2\rangle$ component decreased with time as shown in Figs. 3(b)–3(d), respectively. This decrease can be interpreted by two-body inelastic collisions of $|2, -2\rangle$ with $|2, 0\rangle$, $|2, +1\rangle$, and $|2, +2\rangle$ components because of the large values of $K_2^{(+1,-2)} = 6b_2/7$, $K_2^{(0,-2)} = 4b_2/7$, and $K_2^{(+2,-2)} = 4b_2/7 + 2b_0/5$ from Fig. 1. The dotted and dashed lines are the SMA calculations from Eq. (23) using the measured values of b_0 and b_2 , an average trap frequency of $2\pi \times 82$ Hz, and an average scattering length between spin states. The calculations are in qualitative agreement with the experimental results for all pairs. In particular, for pairs without the $|2, -2\rangle$ component [i.e., the $(2, 0) + (2, -1)$ and $(2, +1) + (2, -1)$ pairs shown in Figs. 3(e) and 3(f), respectively] the SMA calculations with the Thomas-Fermi approximation are in good agreement with the experimental results indicating the prediction of Fig. 1.

However, with regard to the $|2, -2\rangle$ component, the SMA calculations of the $(2, 0) + (2, -2)$, $(2, +1) + (2, -2)$, and $(2, +2) + (2, -2)$ pairs are slightly smaller than the experimental results as shown in Figs. 3(b)–3(d). The decay curves for $(2, +1) + (2, -1)$ and $(2, +2) + (2, -2)$ pairs are theoretically predicted to be identical since $K_2^{(-1,-1)} + K_2^{(+1,-1)} = 4b_2/7 + 2b_0/5$ is equal to $K_2^{(+2,-2)}$. This is also understood from the fact that $|2, +2\rangle + |2, -2\rangle$ is transformed to $|2, +1\rangle + |2, -1\rangle$ by spin rotation. The SMA calculation results for $(2, +1) + (2, -1)$ pair are in good agreement with the experimental results. However, the calculation for the $(2, +2) + (2, -2)$ pair is smaller than the experimental results for trap times longer than 30 ms.

Figure 4 shows relative center-of-mass position in axial direction (z axis) of BECs between different spin states. The center-of-mass position of $m_F = m$ atoms for a trap time t , $z_m(t)$, was measured after Stern-Gerlach separation. The separation between the center-of-mass position of $m_F = m$ and $m_F = m'$ atoms due to the Stern-Gerlach magnetic field is $z_m(0) - z_{m'}(0)$ because two components overlapped at $t = 0$. The relative center-of-mass position for a trap time t shown in Fig. 4 is given by $[z_m(t) - z_{m'}(t)] - [z_m(0) - z_{m'}(0)]$. The magnetic field gradient could be the reason for the difference in the relative center-of-mass positions between different spin states since the low-field- and high-field-seeking states move in opposite directions. The relative center-of-mass position for the $(2, +2) + (2, -2)$ pair shifted to positive values with time while that for the $(2, +1) + (2, -1)$ pair leveled off almost zero. The separation could reduce the inelastic collision loss of the $(2, +2) + (2, -2)$ pair.

The separation may also be caused by mean-field interactions of BECs. The miscibility of multicomponent BECs is determined by s -wave scattering lengths between identical and different spin states. The interaction energy for a mixture of spin m and m' states is given by

$$E_{\text{int}} = \int d\mathbf{r} \left[\frac{g_{mm}}{2} |\psi_m|^4 + \frac{g_{m'm'}}{2} |\psi_{m'}|^4 + g_{mm'} |\psi_m|^2 |\psi_{m'}|^2 \right], \quad (24)$$

where $g_{mm'} = 4\pi\hbar a_{mm'}/M$ with $a_{mm'}$ being the scattering length between m and m' states. $a_{mm'}$ can be expressed in

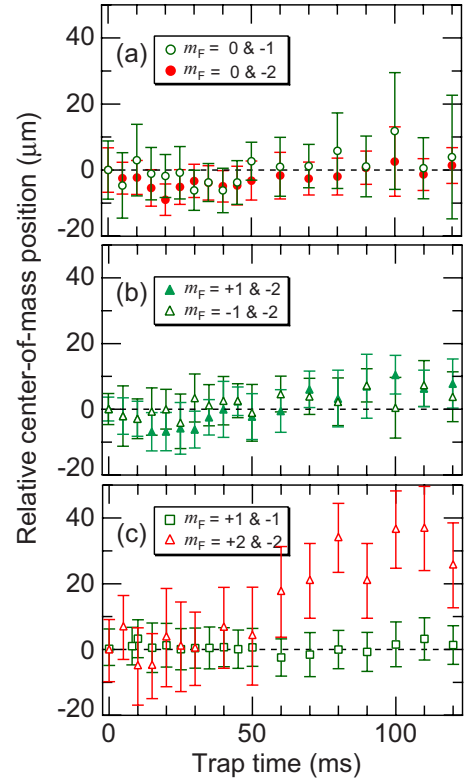


FIG. 4. (Color online) Relative center-of-mass positions of (a) $(2, 0) + (2, -1)$ pair (open circles) and $(2, 0) + (2, -2)$ pair (closed circles), (b) $(2, +1) + (2, -2)$ pair (closed triangles) and $(2, -1) + (2, -2)$ pair (open triangles), (c) $(2, +1) + (2, -1)$ pair (open squares), and $(2, +2) + (2, -2)$ pair (open triangles).

terms of $a_{\mathcal{F}}$ by comparing Eq. (24) and the mean-field expectation value of Eq. (2) for a mixture of m and m' states [21]. Two-component condensates is immiscible when $g_{mm}g_{m'm'} < g_{mm'}^2$. Therefore, based on the measured scattering lengths given in Ref. [8], the $(2, 0) + (2, -1)$ and $(2, -1) + (2, -2)$ pairs are expected to have a phase separation while the other pairs are expected to be miscible.

Figure 5 shows optical densities in the axial direction (z axis) of all spin-state pairs at a trap time of 100 ms, which were averaged in the direction of gravity. These density distributions depend on the spin states of the pairs. Binary BECs of $(2, -1) + (2, -2)$ and $(2, 0) + (2, -1)$ pairs exhibit phase separation and domain formation as shown in Figs. 5(a) and 5(e), due to the immiscibility condition. The $(2, 0) + (2, -2)$ and $(2, +1) + (2, -2)$ pairs exhibit some inhomogeneity between different spin states. The $(2, +2) + (2, -2)$ pair exhibit phase separation despite it being predicted miscible on the basis of Eq. (24) and some other pairs have partial phase separation or homogeneous distribution in Fig. 5. This behavior could be explained by the effects of the magnetic field gradient.

The above analysis demonstrates that it is necessary to consider both the effect of the magnetic field gradient on motions in the FORT and interactions between BECs in the theoretical analysis. We numerically solved GP Eq. (13) with $V_m = V_{\text{trap}} + B' \mu_B m z / 2$, where the field gradient B' in the axial direction was assumed to be 30 mG/cm, the radial (axial)

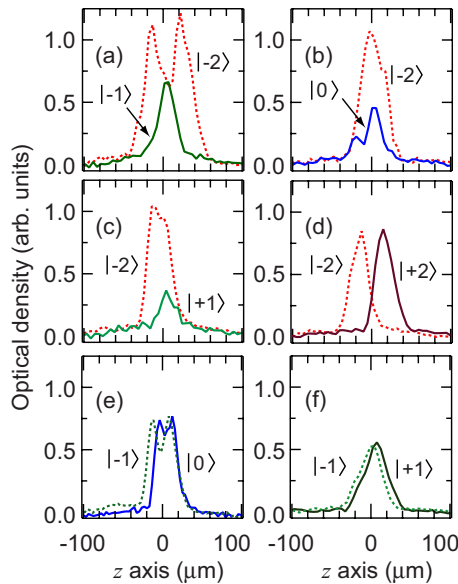


FIG. 5. (Color online) Axial profiles of averaged density distributions for various spin states at an evolution time of 100 ms. Initially populated to (a) $(2,-1)+(2,-2)$, (b) $(2,0)+(2,-2)$, (c) $(2,+1)+(2,-2)$, (d) $(2,+2)+(2,-2)$, (e) $(2,0)+(2,-1)$, and (f) $(2,+1)+(2,-1)$ states with equal population.

trap frequency was $2\pi \times 162$ Hz ($2\pi \times 21$ Hz), and the spin-dependent scattering lengths were derived from Ref. [8]. The results are shown by the solid and dot-dashed lines in Fig. 3. These theoretical results are in good quantitative agreement with the experimental results. The differences between the theoretical and experimental results are significantly reduced for the $(2,-1)+(2,-2)$, $(2,0)+(2,-2)$, and $(2,+2)+(2,-2)$ pairs as shown in Figs. 5(a)–5(d). In particular, the calculation for the $(2,+2)+(2,-2)$ pair can describe reduced atom losses after 50 ms and a kink around 30 ms as shown in Fig. 3(d). However, the measured displacement of the relative center-of-mass position of the $(2,+2)+(2,-2)$ pair cannot be explained by magnetic field gradient alone. We do not have an adequate theory for describing it quantitatively. In the $(2,+1)+(2,-2)$ pair, the theoretical result for $|2,+1\rangle$ atoms cannot completely explain the experimental results, while that for $|2,-2\rangle$ atoms is in better agreement with the experimental results. This may be caused by the inhomogeneous density distribution. The lower atom losses than the SMA calculation is due to the separation of the two components and the suppression of two-body collision between them.

It has been theoretically predicted [20] and experimentally measured [8] that the magnetic phase of a spin-2 ^{87}Rb BEC is in close vicinity to the boundary between the cyclic and antiferromagnetic phases. Saito and Ueda [21] proposed a method to distinguish these two phases. If the magnetic phase is cyclic, a $(2,+2)+(2,-2)$ mixture produces $(2,0)+(2,0)$ pairs, and observation of the $|2,0\rangle$ atoms in the $(2,+2)+(2,-2)$ mixture may be a signature of the cyclic phase. However, the spin-dependent two-body losses are not taken into account in Ref. [21]. To determine the magnetic phase for the upper hyperfine state, it is necessary to take into account the spin-dependent inelastic collision rates [9]. Even

if the $|2,0\rangle$ atoms are produced by the cyclic interaction, the inelastic collision channels of the $(2,0)+(2,+2)$ and $(2,0)+(2,-2)$ states may eliminate the $|2,0\rangle$ atoms, thereby erasing the evidence of the cyclic phase. The obtained collision rates would enable us to quantitatively predict the production rate of $|2,0\rangle$ atoms for the cyclic phase. Another difficulty for determining the magnetic phase is the inhomogeneity of the system. In Ref. [21], it is assumed that all condensates overlap homogeneously over the whole evolution time. However, in the measurement of the $(2,+2)+(2,-2)$ pair, two components were separated in time evolution, as shown in Fig. 5(d). The magnetic phase in the ground state could be determined by spin population measurement when condensate separation is prevented by controlling the magnetic field gradient or applying an additional external field such as optical lattices.

V. CONCLUSIONS

We have studied ultracold two-body inelastic collisions between Zeeman states of $F=2$ atoms both experimentally and theoretically. We measured spin-dependent atom loss rates for all possible combinations of spin states by creating $F=2$ spinor ^{87}Rb BECs in an optical trap and populating the desired Zeeman sublevels by radio-frequency transitions. Atom loss rates were measured at a bias magnetic field of 3.0 G at which spin-exchange collisions are negligible. We show that the two-body inelastic collision rates between all Zeeman sublevels can be expressed in terms of two inelastic collision constants, b_0 and b_2 , which respectively characterize collision channels with total spin 0 (b_0) and total spin 2 (b_2). We have determined these values to be $b_2 = (24.3 \pm 2.4) \times 10^{-14}$ cm³/s, and $b_0 = (9.9 \pm 5.5) \times 10^{-14}$ cm³/s from measured decay rates of single-component BECs (i.e., the $|2,0\rangle$ and $|2,-1\rangle$ states). Observed time evolutions of the atom number for two-component BECs were consistent with SMA calculations using the values of b_0 and b_2 . The discrepancy between the SMA calculations and the experimental results can be explained by spatial separation between two components. The calculated results from the GP equations with a magnetic field gradient were in good agreement with the experimental results.

A detailed understanding of the relative-population dependence and the spin-state dependence of inelastic collisions are key issues in the future study of spinor BECs, such as the determination of the magnetic ground state of spin-2 ^{87}Rb BEC and observation of novel quantum vortices.

ACKNOWLEDGMENTS

We would like to thank T. Kuwamoto, E. Inoue, and Y. Taguchi for experimental assistance and discussions. This work was supported by Grants-in-Aid for Scientific Research (Grant Nos. 17071005, 19740248, and 20540388) from the Ministry of Education, Culture, Sports, Science, and Technology of Japan. Additional funding was provided by CREST, JST.

- [1] As review, J. Weiner, V. S. Bagnato, S. Zilio, and P. S. Julienne, *Rev. Mod. Phys.* **71**, 1 (1999).
- [2] N. N. Klausen, J. L. Bohn, and C. H. Greene, *Phys. Rev. A* **64**, 053602 (2001).
- [3] J. Söding, D. Guéry-Odelin, P. Desbiolles, F. Chevy, H. Inamori, and J. Dalibard, *Appl. Phys. B: Lasers Opt.* **69**, 257 (1999).
- [4] A. Robert, O. Sirjean, A. Browaeys, J. Poupard, S. Nowak, D. Boiron, C. I. Westbrook, and A. Aspect, *Science* **292**, 461 (2001).
- [5] A. Görlitz, T. L. Gustavson, A. E. Leanhardt, R. Löw, A. P. Chikkatur, S. Gupta, S. Inouye, D. E. Pritchard, and W. Ketterle, *Phys. Rev. Lett.* **90**, 090401 (2003).
- [6] T. Kuwamoto, K. Araki, T. Eno, and T. Hirano, *Phys. Rev. A* **69**, 063604 (2004).
- [7] H. Schmaljohann, M. Erhard, J. Kronjäger, M. Kottke, S. van Staa, L. Cacciapuoti, J. J. Arlt, K. Bongs, and K. Sengstock, *Phys. Rev. Lett.* **92**, 040402 (2004).
- [8] A. Widera, F. Gerbier, S. Fölling, T. Gericke, O. Mandel, and I. Bloch, *New J. Phys.* **8**, 152 (2006).
- [9] S. Tojo, A. Tomiyama, M. Iwata, T. Kuwamoto, and T. Hirano, *Appl. Phys. B: Lasers Opt.* **93**, 403 (2008).
- [10] C. J. Myatt, E. A. Burt, R. W. Ghrist, E. A. Cornell, and C. E. Wieman *Phys. Rev. Lett.* **78**, 586 (1997); G. Modugno, G. Ferrari, G. Roati, R. J. Brecha, A. Simoni, and M. Inguscio, *Science* **294**, 1320 (2001).
- [11] T. Isoshima, M. Okano, H. Yasuda, K. Kasa, J. A. M. Huhtamäki, M. Kumakura, and Y. Takahashi, *Phys. Rev. Lett.* **99**, 200403 (2007).
- [12] D. S. Hall, M. R. Matthews, J. R. Ensher, C. E. Wieman, and E. A. Cornell, *Phys. Rev. Lett.* **81**, 1539 (1998).
- [13] K. M. Mertes, J. W. Merrill, R. Carretero-González, D. J. Frantzeskakis, P. G. Kevrekidis, and D. S. Hall, *Phys. Rev. Lett.* **99**, 190402 (2007).
- [14] M. Ueda and M. Koashi, *Phys. Rev. A* **65**, 063602 (2002).
- [15] C. W. Gardiner and P. Zoller, *Quantum Noise*, 2nd ed. (Springer, Berlin, 2000).
- [16] S. Friebe, C. D'Andrea, J. Walz, M. Weitz, and T. W. Hänsch, *Phys. Rev. A* **57**, R20 (1998).
- [17] D. M. Stamper-Kurn, M. R. Andrews, A. P. Chikkatur, S. Inouye, H.-J. Miesner, J. Stenger, and W. Ketterle, *Phys. Rev. Lett.* **80**, 2027 (1998).
- [18] M.-O. Mewes, M. R. Andrews, D. M. Kurn, D. S. Durfee, C. G. Townsend, and W. Ketterle, *Phys. Rev. Lett.* **78**, 582 (1997).
- [19] H. Schmaljohann, M. Erhard, J. Kronjäger, K. Sengstock, and K. Bongs, *Appl. Phys. B: Lasers Opt.* **79**, 1001 (2004).
- [20] C. V. Ciobanu, S.-K. Yip, and Tin-Lun Ho, *Phys. Rev. A* **61**, 033607 (2000).
- [21] H. Saito and M. Ueda, *Phys. Rev. A* **72**, 053628 (2005).